Analytica Chimica Acta 1146 (2021) 155–165

Contents lists available at ScienceDirect

Analytica Chimica Acta

journal homepage: www.elsevier.com/locate/aca

Layer-by-layer assembly strategy for fabrication of polydopamine-polyethyleneimine hybrid modified fibers and their application to solid-phase microextraction of bioactive molecules from medicinal plant samples followed by surface plasmon resonance biosensor validation

Yi Tao *, Lin Chen , Enci Jiang

College of Pharmaceutical Science, Zhejiang University of Technology, Hangzhou, 310032, China

HIGHLIGHTS

- A new PVDF@polydopamine@polyethyleneimine@xanthine oxidase fiber was fabricated.
- The fabricated fibers exhibited highly desired extraction performance.
- The fabricated fibers were applied to real medicinal plants samples.

GRAPHICAL ABSTRACT

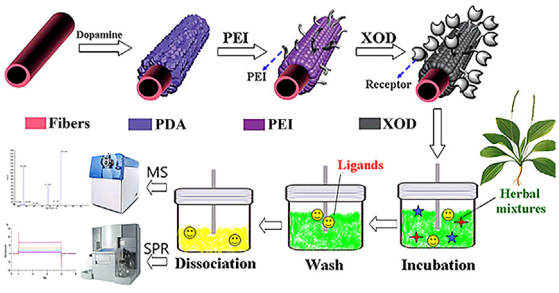

ARTICLE INFO

Article history:
Received 18 August 2020
Received in revised form
10 November 2020
Accepted 13 November 2020
Available online 18 November 2020

Keywords:
Layer-by-layer assembly
Polyvinylidene fluoride fibers
Polydopamine
Polyethyleneimine
Solid-phase microextraction

ABSTRACT

A solid-phase microextraction method is introduced to overcome limitations of classical phytochemical pattern of identifying bioactive compounds, including tedious and time-consuming separation and purification step and consumption of large amounts of organic solvents, which was non-environmentally-friendly. In this proposed method for solid-phase microextraction, polyvinylidene fluoride fibers@polydopamine@polyethyleneimine@receptor as a solid part of the extractors were pushed into sample solution of medicinal plants, and the procedure was followed by stirring and easily dissociation of receptor binding ligands in organic solvent through pulling out of the functionalized fibers. Xanthine oxidase was chosen as the model receptor, while isoacteoside was selected as the model inhibitor. Several effecting parameters were optimized by experimental design, including temperature, ion strength and pH. Nine bioactive components were obtained from extract of *Plantago depressa* by using the established solid-phase micro-extraction method. The limit of detection and limit of quantification of the nine components ranged from 0.0008 to 0.03 mg mL^{-1} and from 0.001 to 0.016 mg mL^{-1}, respectively. The RSD values of intra-day and inter-day precisions ranged from 0.24% to 2.19% and 0.62%–2.84%, respectively. The average recoveries of the nine components were from 95.06 to 104.03% with relative standard deviation (RSD) values from 1.02 to 2.90% for *Plantago depressa*. The RSD values of stability of the nine components ranged from 1.36% to 2.74%, which satisfied the requirements of an analytical method. In addition, surface plasmon resonance biosensor was utilized to corroborate the binding affinity between these compounds and receptor. The avidity values of these ligands corresponded well

* Corresponding author. College of Pharmaceutical Science, Zhejiang University of Technology, 18 Chaowang Avenue, Hangzhou, 310032, China.
E-mail address: taoyi1985@zjut.edu.cn (Y. Tao).

https://doi.org/10.1016/j.aca.2020.11.016

with their IC_{50} values. The results confirmed that polydopamine and polyethyleneimine hybrid modified polyvinylidene fluoride fibers based solid-phase microextraction method was successfully utilized for locating bioactive compounds of medicinal plants.

1. Introduction

Traditional phytochemical pattern of identifying bioactive compounds, which consists of tedious separation and purification steps, consumes several months of time and yields a lot of organic wastewater, cannot meet the green and environmentally-friendly requirements of pharmaceutical industry in the new stage [1]. Thus, solid-phase microextraction (SPME) is introduced due to the reduced operation times and low reagent consumptions. SPME has been applied in various analytical fields such as environmental [2–4] and food analysis [5], bioanalysis [6], etc. Among them, affinity SPME is more interesting to us [7,8]. For affinity SPME, the receptor or antibody are immobilized onto the surface of a modified fiber or capillaries. Reactive groups of receptor or antibody form linkages with the solid support. The receptor–ligand or antibody-antigen interaction is specific, which leads to the extraction of the desired compounds from the sample.

In the current, a plethora of modifications to the SPME technique were developed to adapt the SPME procedure to receptors. For instance, polydopamine (PDA) has received more and more attention as it exhibits a strong adhesive property to many materials through spontaneous oxidative self-polymerization [9]. PDA layer could be utilized for secondary immobilization reactions since it contains functional groups which can be fabricated with various biomolecules, such as proteins, and enzymes etc. via Michael addition or Schiff base formation. Thus, PDA was widely used for the biomimetic surface modification. Polyethylenimine (PEI) is a cationic polymer, which contains the amine group and two carbon aliphatic CH_2CH_2 spacers [10]. The negatively charged receptors will be easily bound to fibers coated with PEI.

Herein, as a showcase, we proposed the layer-by-layer assembly strategy for preparing PVDF fibers@PDA@PEI@receptors for efficient SPME of xanthine oxidase (XOD) binding ligands from medicinal plant samples. The schematic of fabrication of the functionalized PVDF fibers for SPME of XOD inhibitors (XOIs) from herbal mixtures is present in Fig. 1. XOIs are typically used for treating nephropathy and renal stone diseases linked to hyperuricemia. In addition, in order to cross-validate the results, surface plasmon resonance biosensor (SPR) [11,12] are utilized for probing the interaction between XOD and ligands. Avidity value (pD2) of these ligands are calculated and plotted against their IC_{50} values.

2. Experimental

2.1. Reagents

XOD (from bovine milk, EC:1.1.3.22), dopamine hydrochloride (DA), polyethyleneimine (PEI, 25 kDa), EDC, NHS and ethanolamine hydrochloride (ETA) were obtained from Sigma Co. Allopurinol was supplied by Aladdin Bio- Chem Technology Co. Anti-xanthine oxidase antibody (rabbit polyclonal) was purchased from Bioss Biotechnology Co. Polyvinylidene fluoride fibers (PVDF) were purchased from H-Filtration Membrance Technology & Engineering Co. The rhizome of Plantago depressa was obtained from Qingyang City, Gansu Province, and authorized by Prof. Cai Baochang. Voucher specimens were stored in the Zhejiang University of Technology (No. PD161104). FITC-labeled goat anti-rabbit IgG (H + L) antibody was obtained from Rongbai Bio-technology Co. Standard substances, including forsythoside C, isoplantamajoside, plantamajoside, luteolin-7-diglucuronide, isoacteoside, acteoside and scutellarin A were supplied by Weikeqi Bio-technology Co. Vanillic acid was purchased from Yuanye Biological Technology Co. All solutions were prepared by using ultrapure water.

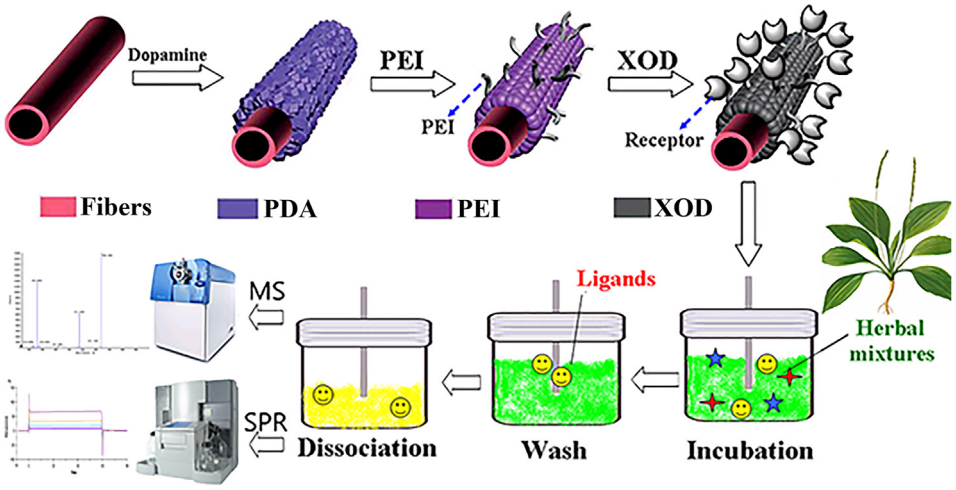

Fig. 1. Schematic of fabrication of the functionalized PVDF fibers for SPME of bioactive compounds from medicinal plants mixture. First, the PVDF@polydopamine @polyethyleneimine@XOD fibers was fabricated by using layer-by-layer assembly strategy. Then, the functionalized fibers were pushed into sample solution of *Plantago depressa* and incubated for a period. Finally, the functionalized fibers were washed for several times and immersed into organic solvent followed by stirring and easily dissociation of receptor binding ligands, which were sent for UPLC-Q-TOF/MS analysis and SPR biosensing.

2.2. Apparatus

The XOD immobilization device was home-made. An intelligent thermostatic water bath was used for controlling the temperature. The apparatus for morphology characterization of PVDF@PDA@PEI@XOD fibers included scanning electron microscope (SEM, Hitachi S4800), and attenuated total reflectance infrared spectroscopy (ATR-IR, Bruker Optics). X-ray photoelectron spectroscopy (XPS) measurements were performed on a Thermo Fisher EscaLab Xi + at a 01 angle of emission using a monochromatic Al Ka source (Ephoton = 1486.6 eV) with a 16 mA filament current and a 12.5 keV filament voltage source energy. The passing energy for the full spectrum and narrow spectrum was set to 100 eV and 30 eV, respectively. The fabricated PVDF fibers were incubated with antibody and detected by fluorescence microscopy (Carl Zeiss, Thornwood, NY). Chemical constituents in medicinal plant samples were profiled by using an UHPLC system (Shimadzu) coupled with a Q-TOF 5600-plus mass spectrometer (AB Sciex). A Synergy 2 multimode reader (Biotek) was used for calculating IC_{50} values. BIAcore T200 system (GE Healthcare) equipped with HC200 M chip (Linear polycarboxylate hydrogel, 200 nm thickness) was employed for probing the interactions between XOD and binding ligands.

2.3. Fabrication of PVDF@PDA@PEI@XOD fibers

The homemade chamber is displayed in Figure S1. A bundle of PVDF fibers (50 fibers, each 5 cm) was immersed into 12 mL Tris-HCl (10 mM, pH 8.5) and ultrasounded for half an hour. After that, 80 mg of dopamine was accurately weighed and added into the chamber. The solution was stirred for an overnight to obtain PVDF@PDA fibers. The PVDF@PDA fibers were then washed with ultrapure water for three times and suspended in 12 mL of PEI (20 mg mL^{-1}). The solution was stirred for 2 h to yield PVDF@PDA@PEI fibers. Subsequently, XOD solutions (1.0 mg/mL) were prepared by adding appropriate amounts of XOD powder to phosphate buffer. 12 mL volume of XOD solution was added to the chamber. Different numbers of PVDF@PDA@PEI fibers (50, 100, 200) were immersed into the XOD solution and then stirred gently for a period. 20 μL solution from the chamber was taken at different time points. Protein content of the solution was determined by using Bradford method.

2.4. Characterization of PVDF@PDA@PEI@XOD fibers

The surface of blank and modified PVDF fibers were characterized by SEM and ATR-IR. The surface element of blank and modified PVDF fibers were detected by using X-ray photoelectron spectroscopy (XPS). Fluorescence microscope was used to visualize distribution of XOD at the surface of PVDF@PDA@PEI@XOD fibers. Both blank PVDF fibers and PVDF@PDA@PEI@XOD fibers were incubated with *anti*-XOD antibody for 24 h. Then, the blank PVDF fibers and PVDF@PDA@PEI@XOD fibers were washed with T-PBS for 3 times. After that, the secondary antibody was added to incubate with the blank PVDF fibers and PVDF@PDA@PEI@XOD fibers for 2 h. Subsequently, T-PBS was used for washing the fibers for 3 times. The blank PVDF fibers and PVDF@PDA@ PEI@XOD fibers were put on a slide glass. A Carl Zeiss fluorescence microscope was applied to monitor fluorescence of fluorescein isothiocyanate (525/530 nm).

2.5. Optimization conditions for the SPME method

All experiments were carried out in the chamber. The model compound isoacteoside (1.0 mL, 1.0 mg mL^{-1}) and 10 PVDF@PDA@PEI@XOD fibers were incubated in a PBS solution (final volume, 12 mL) at proper temperature for a proper time. Then, ten PVDF@PDA@PEI@XOD fibers were left in the chamber and 12 mL of washing solvent was added into the chamber to remove unspecific binding ligands for several times. A magnetic stirrer was put into the chamber to facilitate the washing process. Then, the PVDF@PDA@PEI@XOD fibers were pulled out and transferred to a 2 mL tube. 2 mL of organic solvent was added into the tube to dislodge binding ligands, which were sent to UHPLC-Q-TOF/MS for analysis.

Three affecting factors were optimized by using single factor analysis. First, a series of wash times (one to four times) was optimized in order to rule out unspecific binding compounds. Second, six different proportions of acetonitrile–water and six different proportions of methanol-water (10%, 30%, 50%, 70%, 90% and 100% v/v), were chosen as denature solvents and investigated. Third, five incubation time (5 min, 10 min, 20 min, 30 min and 45 min) were interrogated in order to select a proper time.

The other three factors including temperature (X_1), pH (X_2) and ion strength (X_3) are optimized by using Box–Behnken design. Peak area of isoacteoside is assigned as the dependent variable. The details of experimental design are summarized in Table S1.

2.6. Validation of SPME method

The SPME method was performed as described above. The specificity of the SPME method was corroborated by detecting the interference of negative compound (vanillic acid, 0.1 mg mL^{-1}) at the retention times of the positive compound (isoacteoside, 0.1 mg mL^{-1}). The linearity was analyzed by plotting the peak area of the nine analytes against a series of concentrations (0.006–1.00 mg mL^{-1} for forsythoside C, 0.003–1.00 mg mL^{-1} for isoplantamajoside, 0.003–1.00 mg mL^{-1} for plantamajoside, 0.002–1.00 mg mL^{-1} for luteolin-7-diglucuronide, 0.003–1.00 mg mL^{-1} for isoacteoside, 0.001–1.00 mg mL^{-1} for scutellarin B, 0.016–0.80 mg mL^{-1} for acteoside, 0.001–1.00 mg mL^{-1} for scutellarin A, 0.002–1.00 mg mL^{-1} for hispidulin-7-*O*-β-D-glucuronide). LLOQ was determined as the analytical concentration at a S/N ratio of 10. The intra- and inter-day precision of the method were performed by repeated analyzing standard samples (n = 6) on the same day or on three consecutive days. The repeatability was interrogated by analyzing the same sample for six times. The recovery of the SPME method was carried out by analyzing the peak area of nine analytes (low, medium, high concentration) spiked extract of *Plantago depressa* and the peak area of nine analytes in routine extract of *Plantago depressa*. Stability study was performed with sample solution at 0, 2, 4, 8, 16, 24 h. Variations were expressed by relative standard deviations (R.S.D.). The analysis was performed on a XBridge-C_{18} column (250 mm × 4.6 mm, 5 μm) at 30 °C. 0.1% Formic acid-water (A) and acetonitrile (B) were selected as the mobile phase at a flow rate of 1 mL/min. The UV spectra were monitored at 280 nm. The initial gradient was 10% B and then increased to 50% B in 15 min. The injection volume was set to 20 μL.

2.7. Applications of SPME method to medicinal plant samples

The rhizome of *Plantago depressa* was ground into powder and sieved. Then, 1.0 g of powder was refluxed in 50 mL of boiling water for 1 h. Third, the extracts were filtered and the filtrate was centrifuged at 13,400 rpm for 10 min. The supernatant of *Plantago depressa* (1.0 mL) and 10 PVDF@PDA@PEI@XOD fibers were incubated in 12 mL of PBS solution (pH 6.83, 335.63 mM) at 35 °C for 20 min. Then, the PVDF@PDA@PEI@XOD fibers were pulled out and washed with the incubation buffer for three times to remove unspecific binding compounds. Finally, the PVDF@PDA@PEI@XOD fibers were washed by using 12 mL of 70% methanol-water to

dislodge binding ligands, 2 μL of which were sent to UHPLC-Q-TOF/MS for analysis at a flow rate of 0.3 mL min^{-1}. The separation gradient was set as below: 0–2 min, 5% B; 2.0–8.0 min, 5–30% B; 8.0–13.0 min, 30–95% B; 13.0–17.0 min, 95–100% B. The acquisition parameters for mass analysis were performed as described before [13].

Extraction yields were determined as the ratio of the concentrations for the analytes (C_t) in the extracted solvent and the initial concentration of the analytes (C_0) in the aqueous sample. Extraction capacity (Q_t) was calculated as $Q_t = C_tV_t/M$, where V_t (mL) is the final volume of the extracted solvent of SPME, M is the mass of 5 cm effective length of PVDF@PDA@PEI@XOD fibers. The carryover was estimated by a triple analysis of blank solution performed immediately after analyzing a matrix containing the highest concentration of analytes.

2.8. XOD inhibitory assay

The inhibitory effects of binding ligands were assessed as below. Allopurinol served as a positive control. A gradient concentration of test compounds was prepared to yield a gradient of concentrations between 1 μM and 200 μM 20 μL of the enzyme solution (1.2 U/L) was added to a 96-well plate. Then, 20 μL of the test compound solution were added to the enzyme solution and preincubated for 30 min at 37 °C. Subsequently, 100 μL of HRP labeled antibody was transferred to each well and sealed for 1 h. Afterwards, the solution in the 96-well plate was discarded. The plate was dried on a water adsorbing paper. 200 μL of wash solution was pipetted into each well and incubated for 1 min. Again, the solution in the 96-well plate was abandoned. The plate was dried on a water adsorbing paper. This procedure was performed for five times. 50 μL aliquots of solution A and 50 μL aliquots of solution B were pipetted into each well and maintained in a dark place for 15 min. After that, 50 μL aliquots of stopping solution was transferred to each well. The plate was sent to record the absorbance (450 nm).

2.9. Surface plasmon resonance

The binding affinity between the positive control allopurinol and nine ligands and XOD were monitored by employing a BIAcore T200 SPR system. A new HC200 M sensor chip was utilized. Before use, the chip was washed using sodium acetate buffer. XOD was immobilized on the sensor chip by employing EDC and NHS as coupling reagents. Briefly, a mixture solution of 0.4 M EDC and 0.1 M NHS were injected (10 μL min^{-1}) onto the surface of chip in order to activate the carboxyl groups for 7 min. After that, XOD solutions (80 μg mL^{-1}) were injected onto the surface of chip. Subsequently, 1.0 M ETA-NaOH (pH 8.5) was injected gently to block activated groups on the chip. Sensorgrams of ligands were acquired as different concentrations of solutions were injected (40 μL min^{-1}) onto the XOD immobilized chip. The association time and dissociation time were set to 7 min and 10 min. Finally, 20 μL of glycine-HCl buffer (10 mM, pH 2.0) was injected and the undissociated ligands were removed from the chip. The experimental data were fitted by using a Langmuir binding model. Equilibrium dissociation constant (KD) were calculated. Avidity index of the ligands were obtained by using the equation: AI = −logKD.

3. Results and discussion

3.1. Morphology characterizations

3.1.1. Characterization of PVDF@PDA@PEI@XOD fibers by using SEM

The morphology of the PVDF fibers, PVDF@PDA fibers, PVDF@PDA@PEI fibers, PVDF@PDA@PEI@XOD fibers were characterized by using SEM. The front and vertical picture of PVDF fibers are present in Fig. 2a–b. The inner diameter and outer diameter of PVDF fibers were measured as 0.9 mm and 1.2 mm, respectively. As is shown in Fig. 2c–f, different surface structures were observed for the fabricated PVDF fibers at different stages, which were different from the smooth surface of PVDF fibers. SEM image in Fig. 2d showed that PVDF fibers was wrapped up by surrounding PDA polymer. As is displayed in Fig. 2e, the surface of PVDF fibers was covered with a layer of dendritic structure, which was ascribed to functionalized PEI. Moreover, SEM analysis indicated the surface of PVDF fibers restored smoothing after XOD immobilization (Fig. 2f).

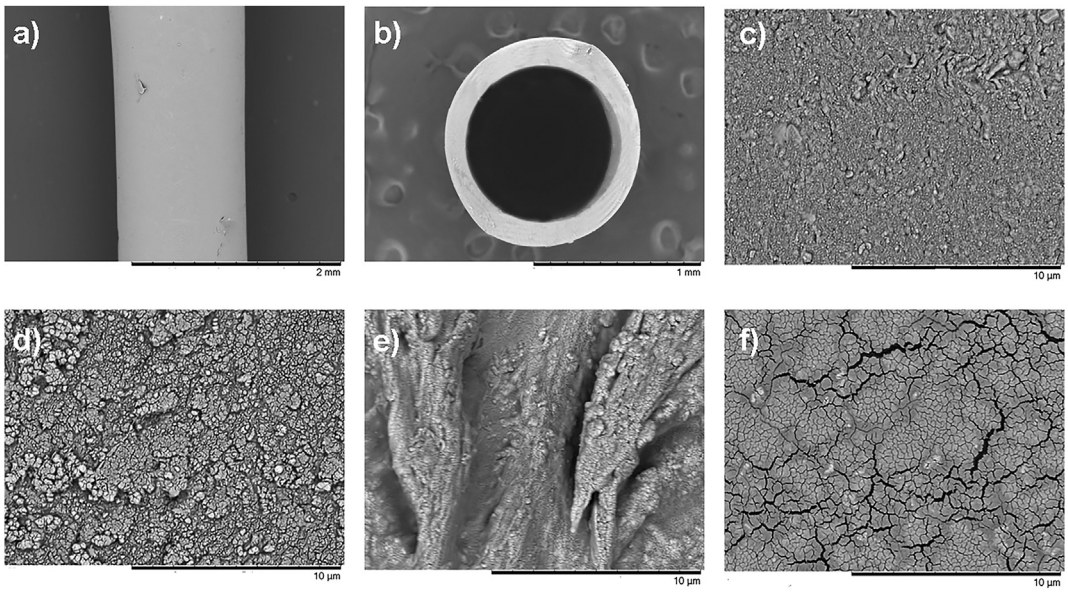

Fig. 2. The front (a), vertical (b), and surface (c) magnification SEM images of a PVDF fiber, SEM images of PVDF@PDA fibers (d), PVDF@PDA@PEI fibers (e) and PVDF@PDA@PEI@XOD fibers (f).

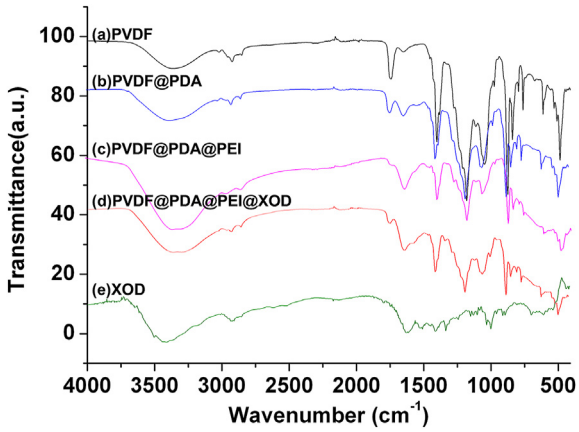

Fig. 3. ATR-IR images of blank PVDF fibers (a), PVDF@PDA fibers (b), PVDF @PDA@PEI fibers (c), PVDF @PDA@PEI@XOD fibers (d) and XOD (e).

3.1.2. Characterization of PVDF@PDA@PEI@XOD fibers by using ATR-IR

The functionalized PVDF fiber was further studied by using ATR-IR. As is shown in Fig. 3a, the peaks around 873 and 1050 cm^{-1} were due to the vibration of β-PVDF. The $-CF_2$ deformation band at 1180 cm^{-1} and $-CH_2$ stretching vibration band at 1402 cm^{-1} were also observed. Surface assembly of PDA on PVDF membrane was evidenced by the ATR-IR data (see Fig. 3b). In comparison with the pristine PVDF, it was obvious that new emerging band at 1637 cm^{-1} was attributed to C=C stretching vibrations of indole and band at 3389 cm^{-1} corresponded to the stretch vibration of N–H of indole. After coating with PEI, the nonaromatic C–N stretching vibrations at 1184 cm^{-1} and 1068 cm^{-1}, and the N–H stretching vibration at 1642 cm^{-1} indicated the existence of the PEI modified PVDF fibers (see Fig. 3c). The absorption bands at 1624 cm^{-1}, 1415 cm^{-1} and 1333 cm^{-1} were regarded as the characteristic absorption bands of the XOD (see Fig. 3d and e). The above results suggested that the PVDF@PDA@PEI@XOD fibers were successfully synthesized.

3.1.3. Characterization of PVDF@PDA@PEI@XOD fibers by using XPS

X-ray photoelectron spectroscopic images of PVDF fibers (A), PVDF@PDA fibers (B), PVDF@PDA@PEI fibers (C) and PVDF@PDA@PEI@XOD fibers (D) are presented in Figure S2. As is displayed in Table S2, the elements of oxygen, carbon and fluorine were observed for blank PVDF fibers. After coating with PDA, the percentage of nitrogen on the surface of PVDF fibers was increased from 0% to 7.84%, whereas the percentage of fluorine was decreased from 37.17% to 0.61%. Apparently, these variations were ascribed to the coating of PDA. As is shown in Table S2, the percentage of nitrogen on the surface of PVDF fibers was increased from 7.84% to 14.19% after coating with PEI. After coating with XOD, the percentage of sulfur on the surface of PVDF fibers was increased from 0% to 0.33%, which may be related to the disulfide bond of the immobilized XOD.

3.1.4. Characterization of PVDF@PDA@PEI@XOD fibers by immunofluorescence

Fluorescence microscopy was utilized to visualize the distribution of XOD at the surface of fabricated PVDF fibers. As is displayed in Fig. 4A, the left image is photographed in order to locate two PVDF fibers. The upper fiber is blank PVDF fiber, whereas the bottom one is PVDF@PDA@PEI@XOD fiber. As is presented in Fig. 4B, the green fluorescence plot clearly revealed the fabricated PVDF fiber in the bottom had been stained with the XOD antibody. It can be seen that XOD was well-distributed at the surface of the fabricated PVDF fiber.

3.2. Optimization conditions for XOD immobilization

Different numbers of PVDF fibers and immobilization time were optimized. The data is shown in Fig. 5. The percentage of immobilized XOD for PVDF fibers ramped up in 1 h and then remained unchanged after 3 h of immobilization. The percentages of immobilized XOD were 59.7%, 52.5% and 49.5% for 200 fibers, 100 fibers and 50 fibers, respectively. Although the largest percentage of immobilization XOD was achieved by using 200 fibers, the largest amount of immobilization protein per fiber was obtained by using

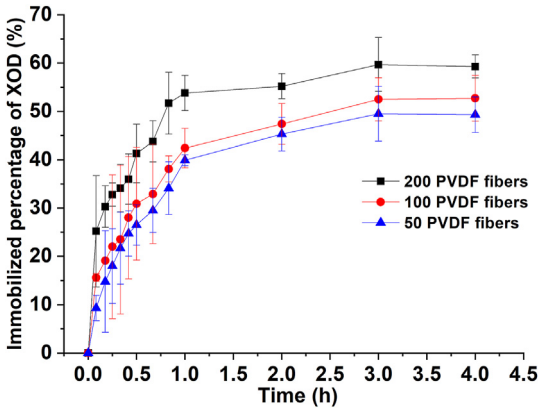

Fig. 5. Curves of immobilized percentage of XOD versus incubation time from 0 h to 4 h.

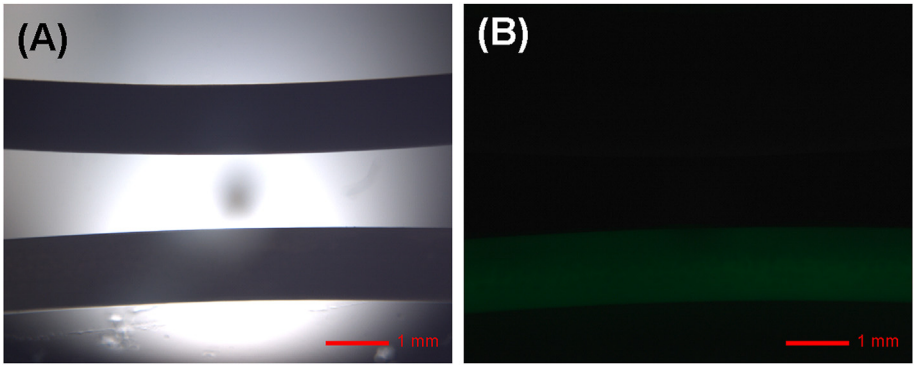

Fig. 4. Light microscopy images (A) and immunofluorescence images (B) of blank (Upper) and functionalized (Lower) PVDF fibers.

50 fibers. Collectively, the immobilization time was set to 3 h and the fibers number was set to 50.

3.3. Optimization conditions for SPME

The washing step plays a crucial role in SPME of XOD binding ligands. Different washing times (1–4 times) were utilized to investigate the nonspecific binding. The data is displayed in Figure S3A. After four times of washing, the peak area of isoacteoside was almost zero. The result revealed that four times were enough for cleaning up all nonspecific binding ligand. The data of wash solvent is present in Figure S3B. The denaturation effect of 70% (v/v) methanol–water was the best and was thus assigned as XOD denaturing solvent. Incubation time is also an important factor affecting the XOD and ligand binding. The data of incubation time is shown in Figure S4. The peak area of isoaceoside reached a plateau in about 20 min. It was speculated that XOD had already been saturated with isoaceoside in 20 min. Therefore, the length of incubation time was set to 20 min.

Temperature, buffer pH and buffer ion strength are the other three important factors that will influence the binding between XOD and ligands. Box–Behnken experimental design are adopted to access to optimal conditions. The data is shown in Table 1 and fitted to a quadratic polynomial model. The value of determination coefficient R^2 (0.9720) demonstrated the observed and the predicted values by the model was consistent.

The interaction between temperature and pH is displayed in Fig. 6A. The incubation system performed well at the middle temperature ranged from 25 °C to 45 °C. The increase of temperature may lower the binding energy between ligand and XOD. But high temperature (>45 °C) may also induce XOD denaturation. The interaction effect between ion strength and temperature is present in Fig. 6B. The distribution of surface charge of XOD could be affected by ionic strength. When the ion strength was increased from 50 to 600 mM, the peak area of isoacteoside arose first and then dropped. The buffer ions play a role in the electrostatic interaction between isoacteoside and XOD. Once exceeding a threshold, the buffer ions can neutralize the surface charge of XOD and weaken the interactions.

The interacting effect of pH and ion strength is demonstrated in Fig. 6C. Among the pH ranging from 6.0 to 8.0, the highest peak area of isoacteoside is observed at the middle of the pH. The XOD (pI 5.3–5.4) have a net negative surface charge, which assists the interaction with isoacteoside (pKa 9.32 ± 0.10) that have positive charge.

The real and predicted peak area of the model are shown in Table S3. The experimental values of peak area were calculated as 813.6 ± 5.9. No significant difference ($p < 0.05$) was observed between the theoretical and experimental responses. Collectively, pH value of buffer was set to 6.83 and incubation time was set to 20 min. Ion strength of buffer was set to 335.63 mM and temperature was set to 35 °C.

3.4. Method validation

In order to investigate the specificity of the method, both positive control isoacteoside and negative control vanillic acid were chosen. The data is present in Figure S5A. Only the peak of isoacteoside was observed (see red line) after SPME. No interference of the negative control vanillic acid was observed. The method showed good specificity. The data of nonspecific binding experiment is shown in Figure S5B. None of isoacteoside and vanillic acid were observed in the chromatogram.

As is shown in Table S4, all calibration curves showed good linearity ($R^2 > 0.9991$). The limit of detection and limit of quantification of these components ranged from 0.0008 to 0.03 mg mL^{-1} and from 0.001 to 0.016 mg mL^{-1}, respectively. The RSD values of intra-day and inter-day precisions ranged from 0.24% to 2.19% and 0.62%–2.84%, respectively (see Table S5). The RSD values of stability of the nine components ranged from 1.36% to 2.74%, which satisfied the requirements of an analytical method. As is displayed in Table S6, the average recoveries of the nine components were from 95.06 to 104.03% with relative standard deviation (RSD) values from 1.02 to 2.90% for *Plantago depressa*. The RSD% values of repeatability of the SPME method was no more than 2.81%. Moreover, the positive control allopurinol was employed to interrogate the method. As is present in Fig. 7A and B, the peak of allopurinol was observed in the dissociated solution after SPME. The MS^1 and MS^2 information of allopurinol (see Fig. 7C and D) was in agreement with that of literature [14]. The extraction yield of allopurinol was obtained as 78% by using the SPME method. Overall, the developed SPME method was sensitive and robust for extracting out of XOD binding ligands.

Table 1
Estimated regression coefficients for the quadratic polynomial model and ANOVA for the experimental results.

Regression coefficients	Value	Standard error	DF	F value	*P*-value Prob > F
X_0	809.06	8.77	9	26.96	0.0001
Linear					
X_1	−5.55	6.93	1	0.6405	0.4998
X_2	−25.51	6.93	1	13.54	0.0079
X_3	−4.74	6.93	1	0.4667	0.5165
Interaction					
X_{12}	−38.98	9.81	1	15.79	0.0054
X_{13}	−24.53	9.81	1	6.25	0.0409
X_{23}	−62.80	9.81	1	41.01	0.0004
Quadratic					
X_1^2	−33.78	9.56	1	12.49	0.0095
X_2^2	−82.71	9.56	1	74.86	<0.0001
X_3^2	−75.55	9.56	1	62.48	<0.0001
Lack of fit			3	7.71	0.0387
Pure error			4		
R^2	0.9720		Adjusted R^2	0.9359	

Standard error: standard deviation that is associated with the mean for this level of the factor; **DF**: degrees of freedom for the term; **Lack of fit**: the variation of the data around the fitted model. If the model does not fit the data well, this will be significant; **Pure error**: the number of replicated design points minus one; **F value**: the test for comparing the variance associated with that term with the residual variance; **R^2**: a measure of the amount of variation around the mean explained by the model; **Adjusted R^2**: a measure of the amount of variation around the mean explained by the model, adjusted for the number of terms in the model. **Prob > F**: probability of seeing the observed F value if the null hypothesis is true.

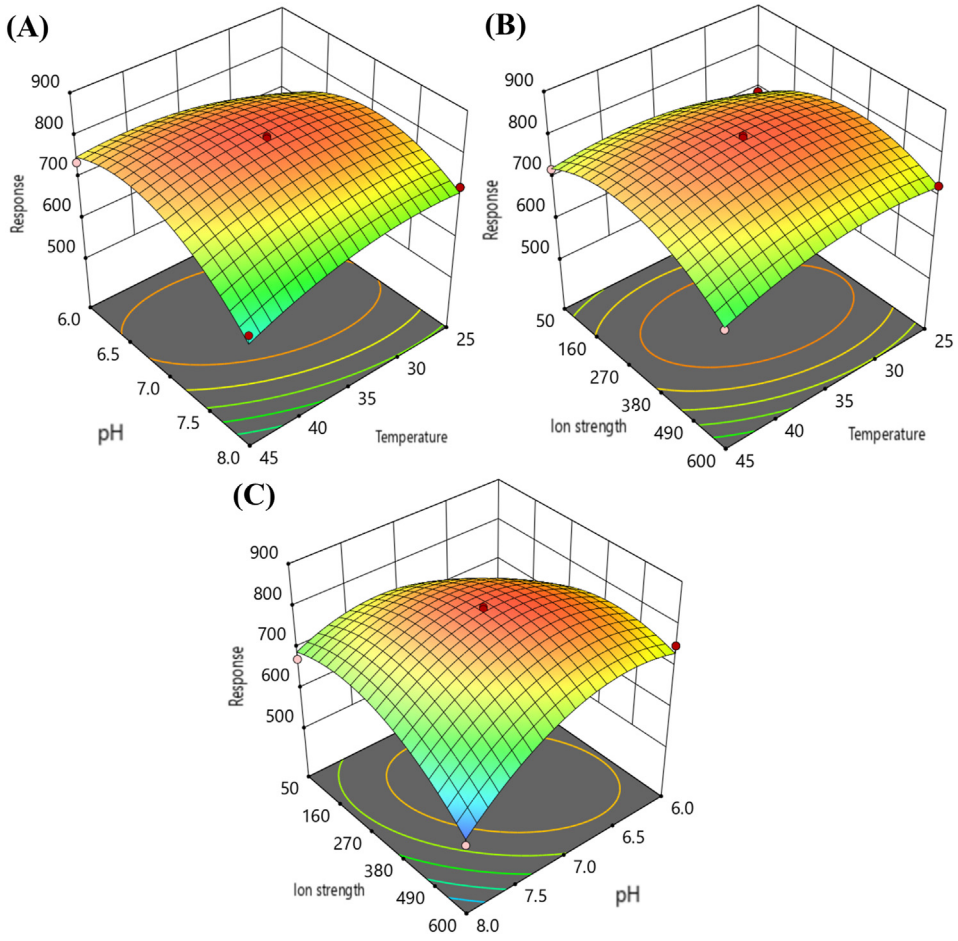

Fig. 6. 3D surface plots showing the interacting effects of three factors. (A) The interaction between pH and temperature, (B) The interaction between ion strength and temperature, (C) The interaction between pH and ion strength.

3.5. Applications to real medicinal plant samples

Characterization of compounds in extract of *Plantago depressa* was conducted by using the UHPLC-Q-TOF-MS method. The total ion current chromatogram (TIC) of *Plantago depressa* is displayed in Fig. 8A. Thirty-four compounds were identified. However, only nine compounds were observed in the dissociated solution by using the SPME method (see Fig. 8B). In order to exclude the nonspecific binding, the TIC of dissociated solution after incubation blank PVDF fibers is presented in Fig. 8C. It can be seen that none of the compounds were bound to the blank PVDF fibers. The retention time and fragmentation information of the nine binding ligands is shown in Table 2. The nine binding ligands (compound **6, 9, 10, 11, 12, 14, 15, 18** and **19)** were plausibly assigned as forsythoside C [15], isoplantamajoside [15], plantamajoside [15], luteolin-7-diglucuronide [16], isoacteoside [17], scutellarin B [18], acteoside [17], scutellarin A [19] and hispidulin-7-*O*-β-D-glucuronide [20] by comparing with that of standard compounds. Chemical structures of the nine ligands are displayed in Figure S6.

As is shown in Table S7, the extraction capacity of the nine analytes ranged from 14.61 μg g^{-1} to 49.24 μg g^{-1}, whereas the extraction yields of the nine analytes were in the range from 17.03% to 92.13%. The carryover of the nine analytes accounted for 0.30%–1.67%, which was negligible. Figure S7 represented the result of reusability of SPME fibers. The extraction yields kept stable after five consecutive cycles and then dropped slightly (ranged from 5.7% to 13.4%) when the cycles increased from six to ten. The reusability of the fabricated SPME fibers was acceptable after ten consecutive cycles.

3.6. XOD inhibitory assay

The IC_{50} value of allopurinol was determined to be 8.36 μM, which was in consistent with the literature [21]. Nine binding ligands were evaluated for their inhibitory effect against XOD. The data are shown in Table 3. Acteoside and scutellarin A exhibited an IC_{50} value of 2.70 μM and 5.26 μM, which were better than that of allopurinol. The XOD inhibitory activities of other seven ligands were increased as follows: forsythoside C, luteolin-7-diglucuronide, hispidulin-7-*O*-β-D-glucuronide, isoplantamajoside, isoacteoside, scutellarin B, and plantamajoside. The XOD inhibitory effect of isoacteoside and acteoside had been reported in the literatures [22]. The XOD inhibitory effects of scutellarin A, plantamajoside, scutellarin B, isoplantamajoside, hispidulin- 7- O-β- D- glucuronide, luteolin-7-diglucuronide and forsythoside C were reported for the first time.

3.7. Surface plasmon resonance

SPR was employed to investigate binding affinity between XOD and the ligands. Binding affinity refers to the strength of the binding between a single biomolecule (such as protein or DNA) and its ligand/binding partner (such as a drug or inhibitor). Binding affinity is generally measured and reported by the equilibrium

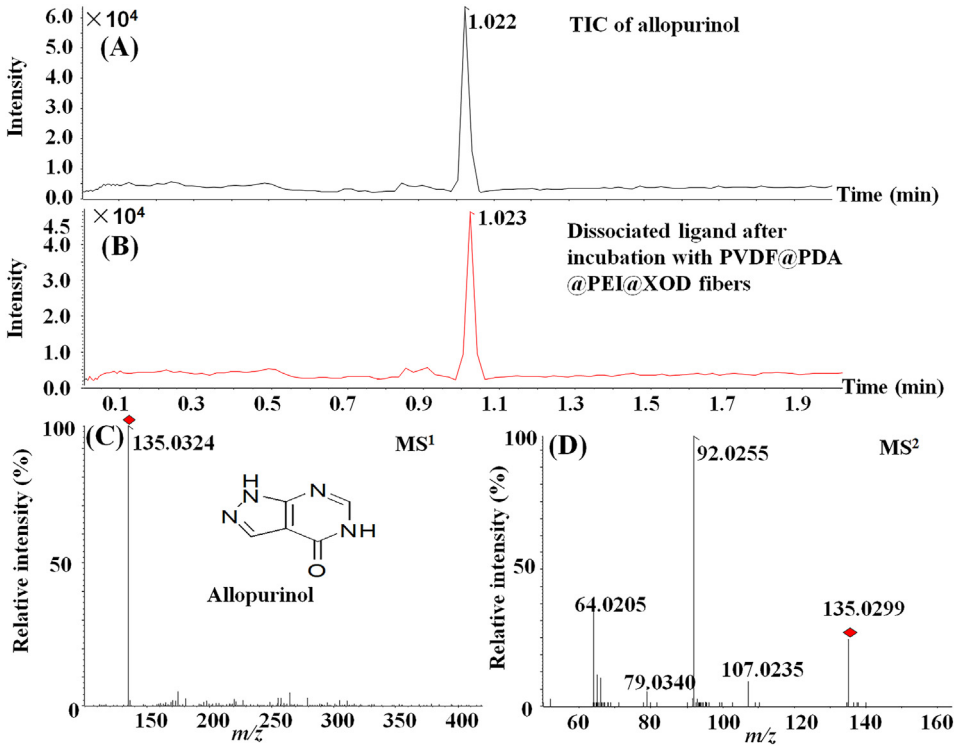

Fig. 7. TIC chromatograms of (A) allopurinol, (B) dissociated solution after incubation with PVDF@PDA@PEI@XOD fibers, (C) MS^1 chromatogram and (D) MS^2 chromatogram of allopurinol.

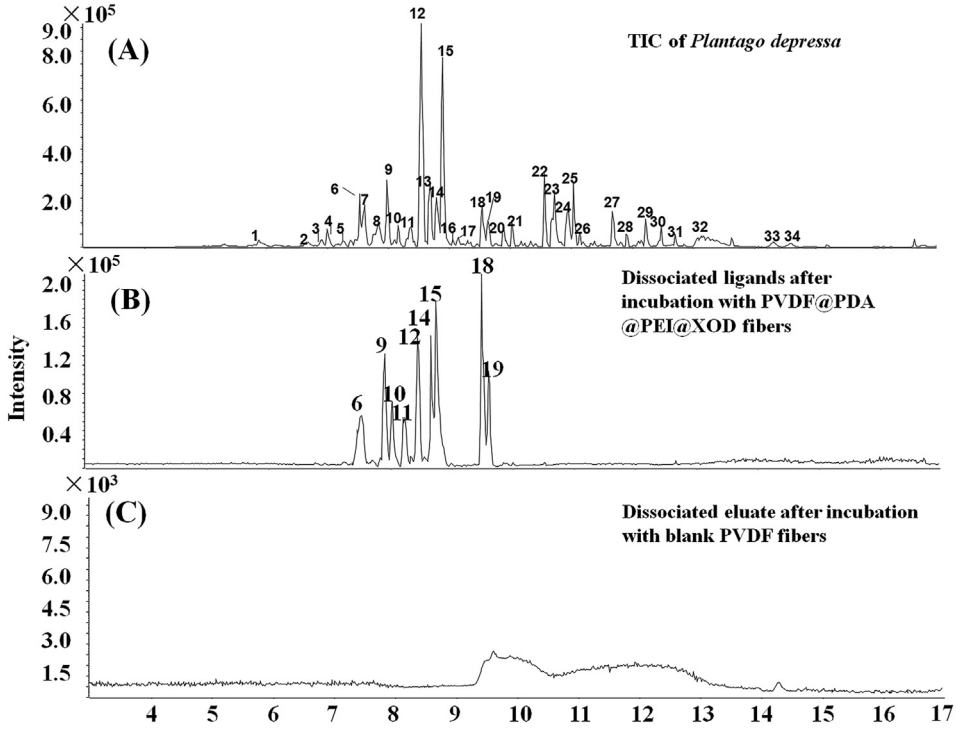

Fig. 8. TIC of crude extract of (A) *Plantago depressa* and (B) dissociated XOD binding ligands after incubation with PVDF@PDA@PEI@XOD fibers or (C) blank PVDF fibers. Peak 6: Forsythoside C, Peak 9: Isoplantamajoside, Peak 10: Plantamajoside, Peak 11: Luteolin-7-diglucuronide, Peak 12: Isoacteoside, Peak 14: Scutellarin B, Peak 15: Acteoside, Peak 18: Scutellarin A, Peak 19: Hispidulin-7-*O*-β-D-glucuronide.

dissociation constant (KD), which is used to evaluate and rank the strength of bimolecular interactions. The smaller the KD value, the greater the binding affinity of the ligand for its receptor. The binding affinity is affected by the interaction between non-covalent bonds, such as hydrogen bonding, electrostatic interaction, hydrophobic force and van der Waals force between two molecules. The

Table 2
Chromatographic and mass spectral characteristics of XOD binding ligands.

No.	t_R (min)	MS^2	Formula	ESI-MS(−)		Identification
				Measured Mass $[M-H]^-$	Error (ppm)	
6	7.543	**621.1854**,529.1576,459.1515,179.0352,161.0250	$C_{29}H_{36}O_{16}$	639.1955	3.8	Forsythoside C
9	8.008	**621.1861**,529.1594,487.1476,323.0789, 251.0570,179.0356,161.0255	$C_{29}H_{36}O_{16}$	639.1952	3.3	Isoplantamajoside
10	8.176	621.1845,477.1630,315.1086,179.0350,**161.0246**,133.0290	$C_{29}H_{36}O_{16}$	639.1960	4.6	Plantamajoside
11	8.362	**461.0734**,285.0401	$C_{27}H_{26}O_{18}$	637.1066	3.1	Luteolin-7-diglucuronide
12	8.548	461.1677,**161.0244**	$C_{29}H_{36}O_{15}$	623.2002	3.3	Isoacteoside
14	8.788	**285.0404**	$C_{21}H_{18}O_{12}$	461.0732	1.4	Scutellarin B
15	8.899	461.1694,**161.0252**	$C_{29}H_{36}O_{15}$	623.2006	3.9	Acteoside
18	9.554	**269.0447**	$C_{21}H_{18}O_{11}$	445.0780	0.8	Scutellarin A
19	9.647	**299.0566**,284.0332	$C_{22}H_{20}O_{12}$	475.0884	0.4	Hispidulin-7-*O*-β-D-glucuronide

Table 3
Inhibitory effects and avidity values of XOD binding ligands.

No.	Compound	IC_{50} (μM) ± SD	pD2
6	Forsythoside C	21.88 ± 1.14	−1.73
9	Isoplantamajoside	11.96 ± 0.83	−1.62
10	Plantamajoside	8.59 ± 0.18	−1.58
11	Luteolin-7-diglucuronide	16.84 ± 0.27	−1.68
12	Isoacteoside	11.51 ± 0.54	−1.60
14	Scutellarin B	9.22 ± 0.93	−1.56
15	Acteoside	2.70 ± 0.29	−0.99
18	Scutellarin A	5.26 ± 0.17	−1.44
19	Hispidulin-7-*O*-β-D-glucuronide	12.08 ± 0.57	−1.64
Control	Allopurinol	8.36 ± 0.34	−1.35

sensorgram between positive inhibitor allopurinol and XOD is displayed in Fig. 9. The KD of allopurinol was determined as 22.63 μM. Besides, the KD values of the nine ligands were in the increasing order: acteoside (9.87 μM) < scutellarin A (27.26 μM) < scutellarin B (36.35 μM) < plantamajoside (38.26 μM) < isoacteoside (40.02 μM) < isoplantamajoside (41.56 μM) < hispidulin-7-*O*-β-D-glucuronide (44.46 μM) < luteolin-7-diglucuronide (48.04 μM) < forsythoside C (53.66 μM). Among the nine ligands, the KD values of acteoside was the lowest. The results demonstrated that the binding affinity of acteoside for XOD was much stronger than that of other eight ligands (see Figure S8). The KD values of isoacteoside, hispidulin-7-*O*-β-D- glucuronide and scutellarin A were determined to be 40.02 μM, 44.46 μM and 27.26 μM, respectively. The binding affinity of scutellarin A is stronger than that of isoacteoside and hispidulin-7-*O*-β-D-glucuronide, which may be ascribed to relatively high of peak 18 in Fig. 8B. In addition, avidity index values of these ligands were calculated by using the formula: AI = −logKD and plotted against their IC_{50} values. As is present in Fig. 10, the larger the avidity index, the lower the IC_{50} value. The avidity index correlated well with IC_{50} values of the ligands. The results revealed that the stronger the binding affinity of ligands for XOD, the better the inhibitory effects.

3.8. Comparisons with previous methods

The developed SPME method was compared with the traditional phytochemical method [23], magnetic beads and ultrafiltration based methods in several terms such as consumption of organic solvent, consumption of time, environmentally friendly and cost (see Table 4). It's obvious that the traditional phytochemical method consumes tons of organic solvent and at least three months. Moreover, the cost of traditional phytochemical method is very high because several kinds of materials (such as Sephadex LH-20 and RP-C_{18} silica gel) are utilized for separation and purification. Magnetic beads based method is another method for locating bioactive molecules. However, the covalent immobilization requires the solvent of glutaraldehyde, which is not environmentally friendly. The immobilization procedure needs a week's time. Moreover, the immobilized receptor may not function well [24]. As for ultrafiltration based method, the cost of ultrafiltration tubes is very expensive. Meanwhile, the soluble receptor is not recyclable [25]. In contrast, the PVDF fibers based SPME is environmentally friendly, recyclable and low-cost, which consumes very little organic solvent and can be accomplished in one week.

4. Conclusion

In this work, the XOD functionalized PVDF fibers was fabricated by using layer-by-layer assembly strategy. Under the optimized conditions, PVDF @PDA@PEI@XOD fibers with high extraction efficiency for isoaceoside was obtained, which was then applied to

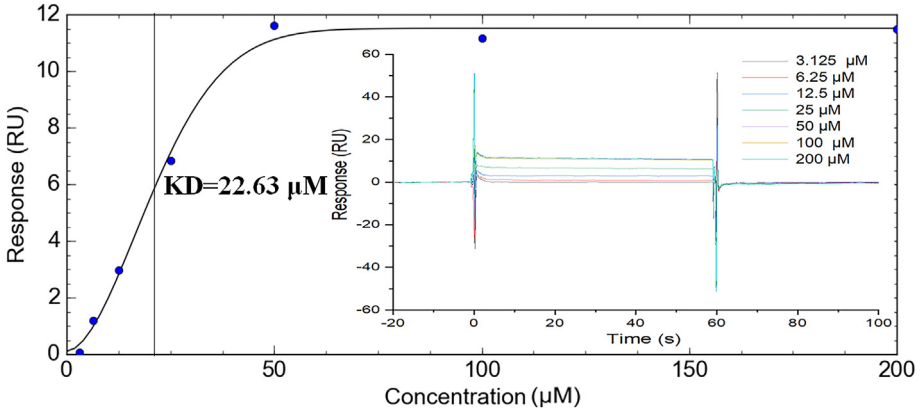

Fig. 9. Measurement of affinity constant KD between the positive control allopurinol and XOD by using SPR affinity analysis.

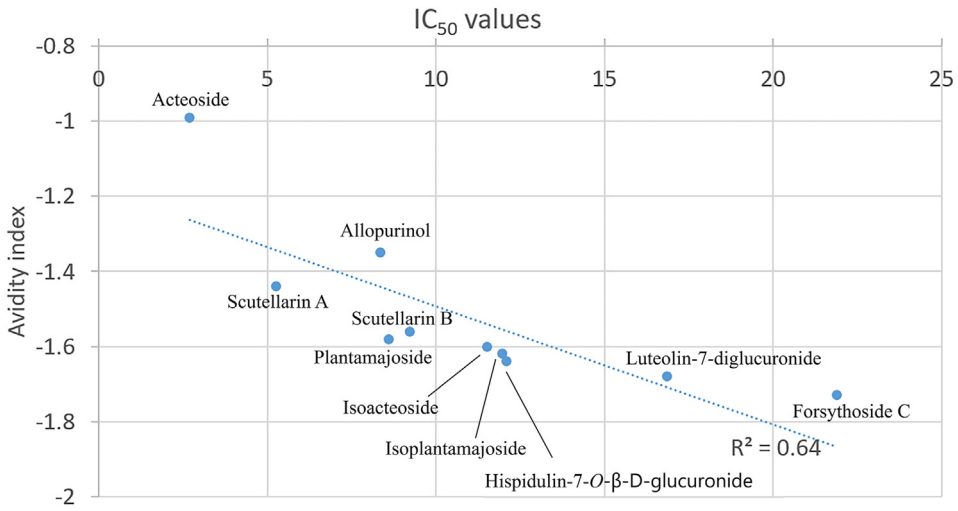

Fig. 10. Plot of avidity index versus IC_{50} values of the nine binding ligands and positive control allopurinol.

Table 4
A comparison between previous methods and PVDF@PDA @PEI@XOD fibers based SPME.

Method	Traditional phytochemical method	Magnetic beads based method	Ultrafiltration method	Fabricated fibers based SPME
Consumption of organic solvent	95% EtOH (15 L) EtOAc (6 L) MeOH, Petroleum ether, Acetone, $CHCl_3$	Gluteraldehyde (1 mL), Acetonitrile	Acetonitrile (no more than 100 mL)	Very little (no more than 100 mL)
Consumption of time	Three months (At least)	More than a week	One week	One week
Environmentally friendly	No	No	Yes	Yes
Cost	Expensive	Expensive	Expensive	Cheap
Receptor function	Function	May not function	Function	Function
Recyclable	No	Yes	No	Yes
Reference	[23]	[24]	[25]	This work

extract XOD binding ligands from crude extract of *Plantago depressa* samples prior to UHPLC-Q-TOF-MS analysis. The developed SPME method showed good performance. It should be noticed that seven new XOD inhibitors were identified by using the SPME method. The modification of PVDF fibers with PDA and PEI provides a new paradigm for identification of bioactive compounds from medicinal plant mixtures. However, the performance of the PVDF @PDA@PEI fibers for other receptors needs to be further studied in order to expand its applications.

CRediT authorship contribution statement

Yi Tao: Conceptualization, Methodology, Supervision, Writing - review & editing. **Lin Chen:** Data curation, Visualization, Investigation, Writing - original draft. **Enci Jiang:** Software, Validation.

Declaration of competing interest

The authors declare that they have no known competing financial interests or personal relationships that could have appeared to influence the work reported in this paper.

Acknowledgements

This study was supported by the National Natural Science Foundation of China (No.81703701) and Natural Science Foundation of Zhejiang Province (No.LY21H280008). The authors would like to thank the anonymous reviewers for their invaluable suggestions that helped improve the manuscript.

Appendix A. Supplementary data

Supplementary data to this article can be found online at https://doi.org/10.1016/j.aca.2020.11.016.

References

[1] Y. Tao, X. Gu, W. Li, H. Wu, B. Cai, B. Zhang, Techniques for biological fingerprinting of traditional Chinese medicine, Trac. Trends Anal. Chem. 97 (2017) 272–282.
[2] S. Liu, H. Yang, S. Yang, Y. Huang, Z. Xiang, G. Ouyang, Carbon dots based solid phase microextraction of 2-nitroaniline followed by fluorescence sensing for selective early screening and sensitive gas chromatography-mass spectrometry determination, Anal. Chim. Acta 1111 (2020) 147–154.
[3] S. Mondal, J. Xu, G. Chen, S. Huang, C. Huang, L. Yin, G. Ouyang, Solid-phase microextraction of antibiotics from fish muscle by using MIL-101(Cr)NH2-polyacrylonitrile fiber and their identification by liquid chromatography-tandem mass spectrometry, Anal. Chim. Acta 1047 (2019) 62–70.
[4] A.R. Ghiasvand, M. Pirdadeh-Beiranvand, Cooling/heating-assisted headspace solid-phase microextraction of polycyclic aromatic hydrocarbons from contaminated soils, Anal. Chim. Acta 900 (2015) 56–66.
[5] S. Dowlatshah, M. Saraji, A silica-based three-dimensional molecularly imprinted coating for the selective solid-phase microextraction of difenoconazole from wheat and fruits samples, Anal. Chim. Acta 1098 (2020) 37–46.
[6] G. Ouyang, D. Vuckovic, J. Pawliszyn, Nondestructive sampling of living systems using in Vivo solid-phase microextraction, Chem. Rev. 111 (2011) 2784–2814.
[7] Y. Tao, J. Yan, B. Cai, Lable-free bio-affinity mass spectrometry for screening and locating bioactive molecules, Mass Spectrom. Rev. (2019), https://doi.org/10.1002/mas.21613.
[8] R. Prudent, D.A. Annis, P.J. Dandliker, J.-Y. Ortholand, D. Roche, Exploring new targets and chemical space with affinity selection-mass spectrometry, Nat. Rev. Chem. (2020), https://doi.org/10.1038/s41570-41020-00229-41572.
[9] Y. Liu, K. Ai, L. Lu, Polydopamine and its derivative materials: synthesis and promising applications in energy, environmental, and biomedical fields, Chem. Rev. 114 (2014) 5057–5115.

[10] J. Li, X. Wang, M. Shen, X. Shi, Polyethylenimine-Assisted generation of optical nanoprobes for biosensing applications, ACS Appl. Bio. Mater. 3 (2020) 3935–3955.
[11] T.-H. Lee, D.J. Hirst, K. Kulkarni, M.P. Del Borgo, M.-I. Aguilar, Exploring molecular-biomembrane interactions with surface plasmon resonance and dual polarization interferometry technology: expanding the spotlight onto biomembrane structure, Chem. Rev. 118 (2018) 5392–5487.
[12] L. Chen, D. Lv, S. Wang, D. Wang, X. Chen, Y. Liu, Z. Hong, Z. Zhu, Y. Cao, Y. Chai, Surface plasmon resonance-based membrane protein-targeted active ingredients recognition strategy: construction and implementation in ligand screening from herbal medicines, Anal. Chem. 92 (2020) 3972–3980.
[13] Y. Tao, S.R. Huang, W.D. Li, B.C. Cai, Simultaneous determination of ten bioactive components in raw and processed Radix *Dipsaci* by UPLC-Q-TOF-MS, J. Chromatogr. Sci. 57 (2019) 122–129.
[14] D.M. Rathod, K.R. Patel, H.N. Mistri, A.G. Jangid, P.S. Shrivastav, M. Sanyal, Simultaneous analysis of allopurinol and oxypurinol using a validated liquid chromatography–tandem mass spectrometry method in human plasma, J. Pharma. Anal. 7 (2017) 56–62.
[15] D. Wang, M. Qi, Q. Yang, R. Tong, R. Wang, S.W.A. Bligh, L. Yang, Z. Wang, Comprehensive metabolite profiling of Plantaginis Semen using ultra high performance liquid chromatography with electrospray ionization quadrupole time-of-flight tandem mass spectrometry coupled with elevated energy technique, J. Separ. Sci. 39 (2016) 1842–1852.
[16] L. Funes, S. Fernández-Arroyo, O. Laporta, A. Pons, E. Roche, A. Segura-Carretero, A. Fernández-Gutiérrez, V. Micol, Correlation between plasma antioxidant capacity and verbascoside levels in rats after oral administration of lemon verbena extract, Food Chem. 117 (2009) 589–598.
[17] L. Zhou, J.-D. Xu, S.-S. Zhou, Q. Mao, M. Kong, H. Shen, X.-Y. Li, S.-M. Duan, J. Xu, S.-L. Li, Integrating targeted glycomics and untargeted metabolomics to investigate the processing chemistry of herbal medicines, a case study on Rehmanniae Radix, J. Chromatogr. A 1472 (2016) 74–87.
[18] T.-L. Wong, Y.-Q. An, B.-C. Yan, R.-Q. Yue, T.-B. Zhang, H.-M. Ho, T.-J. Ren, H.-Y. Fung, D.-L. Ma, C.-H. Leung, Z.-L. Liu, J.-X. Pu, Q.-B. Han, H.-D. Sun, Comprehensive quantitative analysis of Chinese patent drug YinHuang drop pill by ultra high-performance liquid chromatography quadrupole time of flight mass spectrometry, J.Pharm. Biomed. Anal. 125 (2016) 415–426.
[19] V. Šulniūtė, A. Pukalskas, P.R. Venskutonis, Phytochemical composition of fractions isolated from ten Salvia species by supercritical carbon dioxide and pressurized liquid extraction methods, Food Chem. 224 (2017) 37–47.
[20] S. Li, H. Jiang, Z. Lin, S. Deng, Y. Guan, H. Wang, S. Chen, An on-line high-performance liquid chromatography–diode-array detector–multi-stage mass spectrometry–deoxyribonucleic acid–4′,6-diamidino-2-phenylindole–fluorescence detector system for screening the DNA-binding active compounds in Fufang Banbianlian Injection, J. Chromatogr. A 1424 (2015) 37–50.
[21] P. Pacher, A. Nivorozhkin, C. Szabó, Therapeutic effects of xanthine oxidase inhibitors: renaissance half a century after the discovery of allopurinol, Pharmacol. Rev. 58 (2006) 87–114.
[22] J.-X. Zeng, J. Wang, S.-W. Zhang, J.-X. Zhu, M. Li, W.-H. Huang, J.-Y. Wan, H.-Q. Yao, C.-Z. Wang, C.-S. Yuan, Antigout effects of Plantago asiatica: xanthine oxidase inhibitory activities assessed by electrochemical biosensing method, evid-based compl, Alternative 2018 (2018) 1364617.
[23] X.-Q. Song, K. Zhu, J.-H. Yu, Q. Zhang, Y. Zhang, F. He, Z.-Q. Cheng, C.-S. Jiang, J. Bao, H. Zhang, New octadecanoid enantiomers from the whole plants of *Plantago depressa*, Molecules 23 (2018) 1723.
[24] M. Yasuda, D.R. Wilson, S.D. Fugmann, R. Moaddel, Synthesis and characterization of SIRT6 protein coated magnetic beads: identification of a novel inhibitor of SIRT6 deacetylase from medicinal plant extracts, Anal. Chem. 83 (2011) 7400–7407.
[25] Y. Tao, H. Cai, W. Li, B. Cai, Ultrafiltration coupled with high-performance liquid chromatography and quadrupole-time-of-flight mass spectrometry for screening lipase binders from different extracts of Dendrobium officinale, Anal. Bioanal. Chem. 407 (2015) 6081–6093.